Course Modules for Teaching Geological Structures Using Cyber-mapping Three-Dimensional (3D) Photo-realistic Digital Replica of Geological Outcrops in the Arbuckle Anticline, Southern Oklahoma

Mohamed Abdelsalam
Missouri University of Science and Technology
Department of Geological Sciences and Engineering
1400 North Bishop Avenue
Rolla, MO, 65401

Carlos Aiken, Mohammed Alfarhan, Lionel White
University of Texas at Dallas
Department of Geosciences
800 West Campbell Road
Richardson, TX, 75080

May, 2010

To obtain the OpenSceneGraph files, please e-mail Mohamed Abdelsalam at abdelsam@mst.edu

TABLE OF CONTENTS

SUMMARY

This article presents a number of modules that can be used for explaining geological structures using three-dimensional (3D) photo-realistic digital replica (3DR) of geological outcrops in the Arbuckle anticline in southern Oklahoma. The 3DRs were acquired from different parts of the Arbuckle anticline including second order folds and a conjugate set of reverse faults on the southern limb of the anticline, second-order folds and thrusts on the hinge of the anticline, and an angular unconformity on the northern limb of the anticline. These 3DRs were developed using cyber-mapping technology and were used at Missouri University of Science and Technology for explaining the geometry of various geological structures. The models were initially developed in a cyber-mapping format, but to allow other instructors to use them, they were subsequently converted into OpenSceneGraph and 3D Portable Document Format (PDF) files. The OpenSceneGraph files can be displayed and visualized using the GeoWall 3D visualization system whereas the PDF files can be visualized using regular computers and projectors. The document will: (1) Describe cyber-mapping technology. (2) Outline regional setting of the Arbuckle anticline. (3) Outline the geology of the Arbuckle anticline. (4) Describe the geology of the three 3DR models. (5) Present the teaching modules.

CYBER-MAPPING TECHNOLOGY

Cyber-mapping (Xu et al. 1999; Xu, 2000; Alfarhan, 2010) uses the integration of Real Time Kinematic (RTK) Global Positioning System (GPS), Light Detection and Ranging (LIDAR) scanning, digital photography, and geospatial software to produce high spatial resolution three-dimensional (3D) photo-realistic digital replica (3DR) of geological

outcrops. This technology has been used for geological studies (Xu et al., 1999, 2000, 2001; Thurmond et al., 2005; Oldow et al., 2006; Alfarhan et al., 2008; Olariu et al., 2008) and oil and gas exploration and reservoir characterization (Zeng et al., 2005; Bellian et al., 2005; Pringle et al., 2006). The success of cyber-mapping technology lies in: (1) The advances made in GPS technology, now capable of reporting X-Y-Z positioning to cm-scale spatial resolution and accuracy (Parkinson and Spilker, 1996). (2) The efficiency of reflectorless laser-mapping technology where air-borne and terrestrial LIDAR scanners are now capable of capturing thousands of data points per second enabling the creation of Digital Surface Models (DSMs) in cm-scale spatial resolution and accuracy in short time (McCaffrey et al., 2005). Reigl scanners - Z210, Z360 and LPM 3800 AVS are used in this work. (3) The development of effective algorithm for accurate fitting of smooth surfaces onto complex LIDAR data cloud constituting millions of data points. In addition, significant advances have been made in developing algorithms for mapping the pixels of the high spatial resolution photographs onto the complex DSMs without geometrical distortion (Xu et al., 2004). (4) Advances made in 3D visualization hardware and software that now allows literally virtual visits and field trips to geometrical features (Edelson and Gordin, 1998; Hurst, 1998; Kemp, 1999; Marschallinger and Johnson, 2001; Johnson et al., 2006; Kelly and Riggs, 2006). These 3D visualization systems, such as the GeoWall, are now becoming increasingly affordable (Johnson et al., 2006).

In geology, cyber-mapping technology is used to develop DSMs of geological outcrops at cm- to dm-scale spatial resolution and accurately. High spatial resolution digital

photographs are draped onto these DSMs to generate 3DRs that can be viewed in 3D and analyzed for the extraction of accurate geometrical relationships. This technology also allows data to be collected from remote or inaccessible locations, such as on cliff faces.

REGIONAL SETTING OF THE ARBUCKLE ANTICLINE

The Arbuckle anticline is one of three NW-trending anticlines (the Hunton arch and the Tishomingo anticline represent the other two) in the Arbuckle mountains in southern Oklahoma. These structures are part of the NE-trending Paleozoic Appalachian-Ouachita orogenic belt which extends in the eastern and southeastern margin of North America (Figure 1; Thomas, 1993). The organic belt is thought to be the result of the closure of the lapetan ocean during the assembly of super-continent Pangea ~270 Ma resulting in the collision of various arcs, exotic terranes and other continents with the southern margin of Laurentia. Many authors interpreted the zigzag nature of the Appalachian-Ouachita orgoenic belt as mimicking the shape of the lapetan rifted margin with its oceanic spreading centers, transform faults and triple junctions (Figure 1; Thomas, 2004).

The NW trend of the Arbuckle mountains is at right angle to the overall NE trend of the Appalachean-Ouachita orogenic front (Figure 1). This was interpreted as reflecting the geometry of the lapetan rifted margin where an embayment (the Ouachita embayment) extended northwestward from the NE-trending Ouachita rift (Figure 1; Thomas, 1993). The Ouachita embayment was formed in response to the development of a series of NW-tending normal faults (the southern Oklahoma fault system) during the onset of the southern Oklahoma aulacogen (Figure 1).

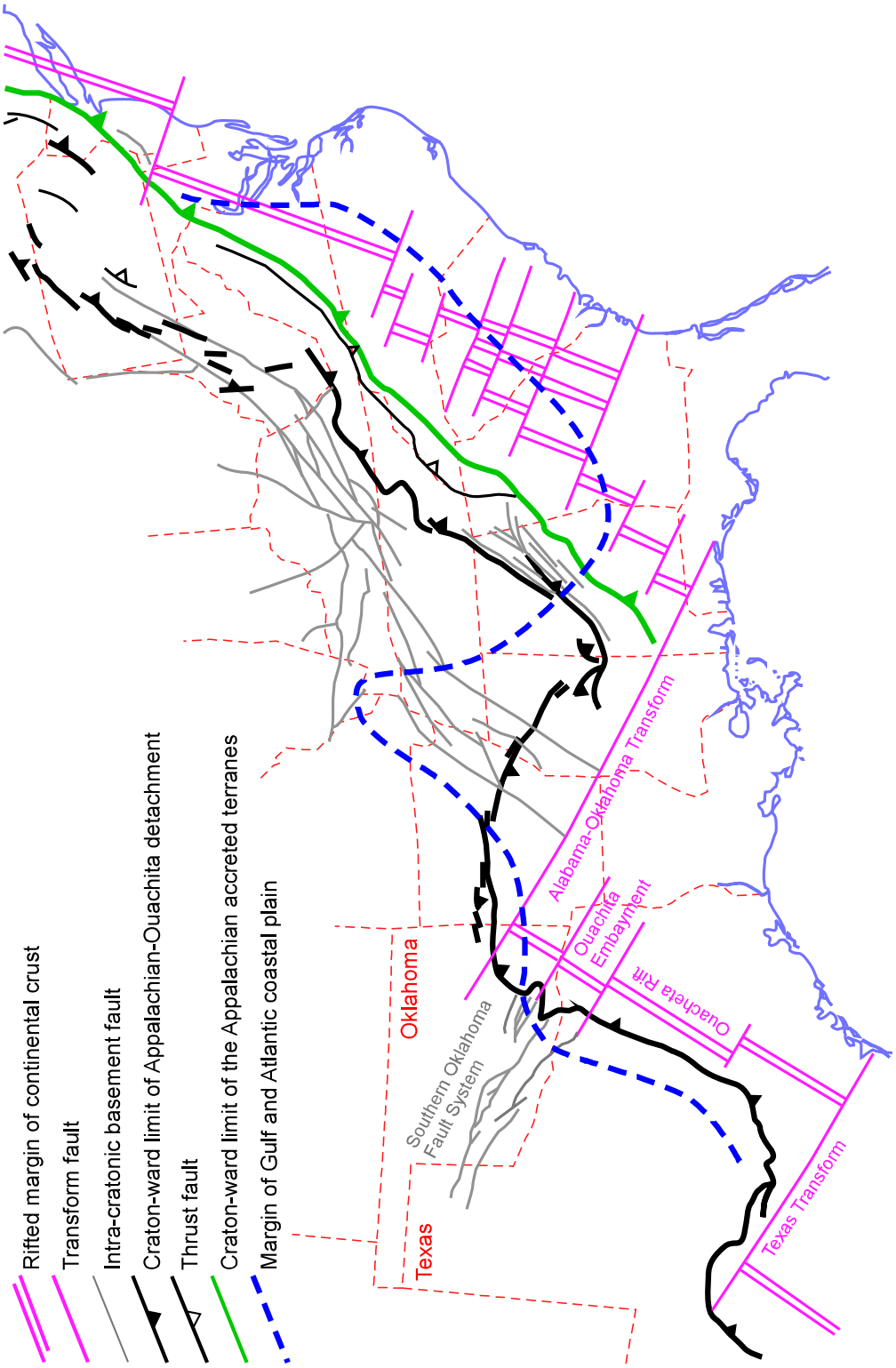

Figure 1: A regional tectonic map of northeastern and southeastern United States showing the location of the Arbuckle Mountains within the Appalachian-Washita orogenic belt as well as tectonic elements of lapetan rifted margin. After Thomas (1993).

GEOLOGY OF THE ARBUCKLE ANTICLINE

The Arbuckle anticline (Figure 2) is a doubly-plunging, NW-trending fold structure in the western part of the Arbuckle mountains in southern Oklahoma. This structure is ~40 km in length and ~15 km across. The anticline was first mapped by Ham and McKinley (1954) and this map was subsequently updated by Johnson (1990). The core of the structure is dominated by the Colbert Rhyolite which is Middle Cambrian in age. These crystalline rocks are followed outward by the Upper Cambrian limestone and dolomite of the Timbered Hill Group and the Butterly dolomite, respectively. The Upper Cambrian rocks give place outward to the Lower Ordovician cherty and sandy limestone of the Cool Creek and McKenzie formations followed by the limestone and dolomite of the Spring Creek and Kindblade formations. Johnson (1990) grouped the Buttery dolomite, and the Cool Creek, the McKenzie Hill, the West Spring, and the Kindblade formations into the Arbuckle group. The lower Ordovician rocks are replaced outward by Middle-Upper Ordovician sedimentary rocks that are divided from older to younger into the Oil Creek and Joins formations, the Bromde, Tulip Creek and McLish formations, the Sylvan shale and the Viola group (Viola group constitutes the Wellings and Viola Springs formations), and the Hunton group which comprises the Frisco, the Bois, the d'Arc, the Haragane and the Henryhouse, the Clarita, the Cochrane, and the Keel formations. The Oil Creek and Joins formations are made up of sandstone in the base overlain by limestone and shale. The Bromde, Tulip Creek and McLish formations are dominated by a succession of sandstone, green shale and limestone. The Sylvan shale and the Viola group comprise shale and limestone. The Hunton group is dominantly limestone and marlstone. Johnson (1990) grouped the Oil Creek, the Bromide, the Tulip Creek and the

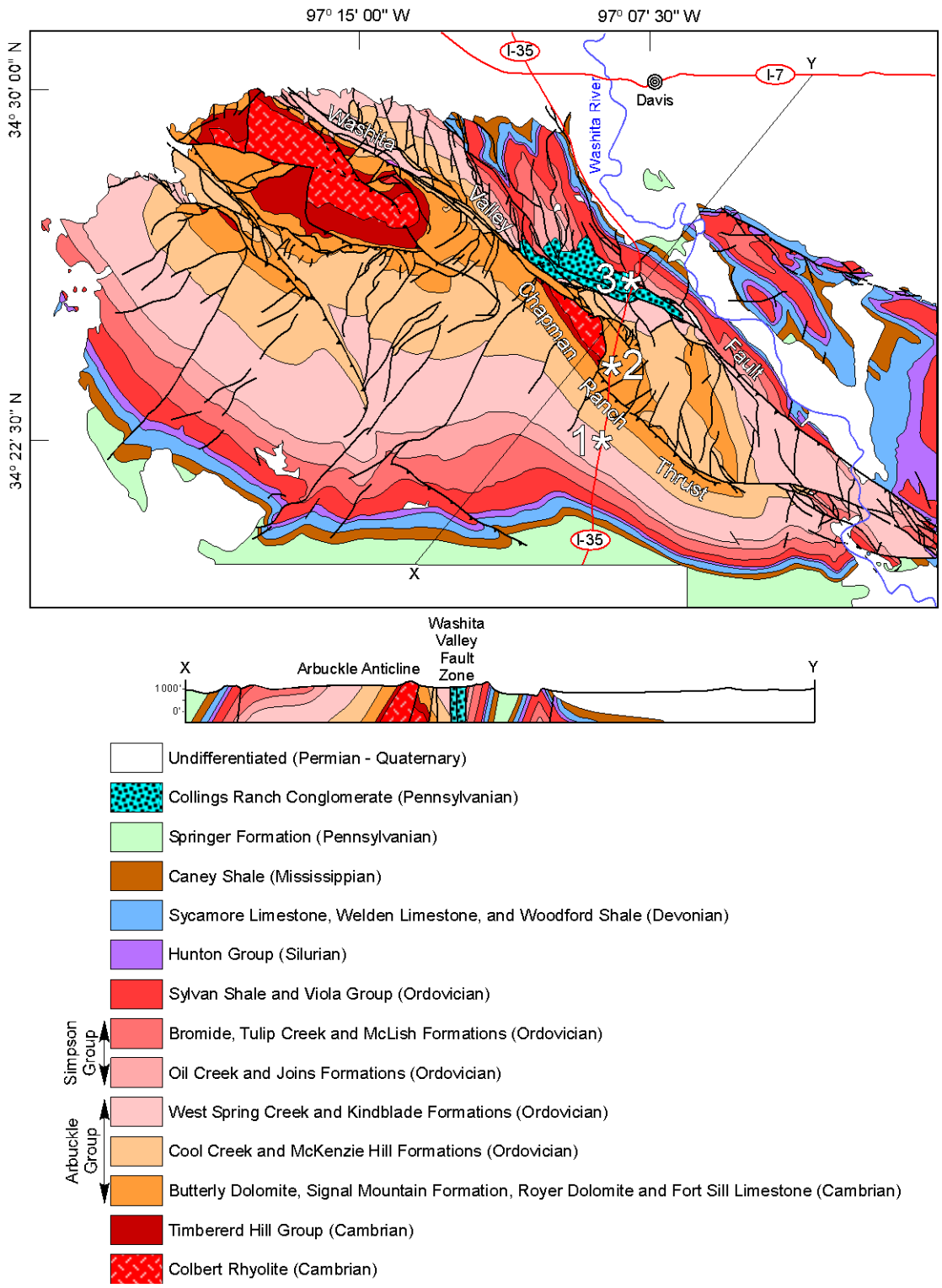

Figure 2: Geological map and cross-section of the Arbuckle anticline. After Ham and McKinley (1954) and Johnson (1990). The locations of the three 3DR outcrops are shown in red dots.

McLish formations into the Simpson group. The Middle-Upper Ordovician rocks are followed outward by the Mississippian-Devonian sedimentary rocks of the Sycamore limestone, the Welden limestone and the Woodford shale. These are followed by the Mississippian-age Caney shale. The steeply dipping to the north Sylvan shale and the Viola group on the northern limb of the Arbuckle anticline are overlain by the almost horizontal Pennsylvanian-age Collings Ranch conglomerate in an angular unconformity field relationship. This conglomerate is a clast-supported and it is dominated by boulder to pebble-size limestone clasts.

The Arbuckle anticline is deformed by a number of NW-trending faults that seems to increase in intensity in the northeastern limb of the anticline (Figure 2). NE-trending faults are also present. The most important NW-tending faults that are relevant to understanding the geological setting of the three 3DR models are the NW-trending Chapman Ranch fault and the Washita Valley fault zone (Figure 2). Johnson (1990) interpreted the Chapman Ranch fault as a NE-verging thrust dominantly within the Upper Cambrian Butterly dolomite to the southwest of the anticline core which is dominated by the Middle Cambrian Colbert rhyolite (Figure 2). Northeast of the anticline core is the exposure of the complex NW-trending Washita Valley fault zone (Figure 2). The southeastern segment of this fault zone was mapped by Johnson (1990) as a thrust fault. However, the geological cross-section which accompanied the geological map of Johnson (1990) suggests that the northwestern segment of the Washita Valley fault zone is dominated by a normal-slip displacement forming, in some places, graben structures within which the Collings Ranch conglomerate was deposited. These differences in the

interpretation of the Washita Valley fault zone not only highlight possible along-strike and structural level variation, but also the uncertainties regarding the nature of this fault zone (normal, thrust, strike-slip). The nature of the fault has been debated since the beginning of the last century (see for example Tanner III (1967) for various interpretations of the fault in the literature of the first half of the twentieth century). This debase seemed to settle towards considering the Washita Valley fault zone as a left-lateral strike-slip fault with ~60 km displacement (see summary in Wilkinson (1997). However, both Palladino (1986) from surface geology observations and Wilkinson (1997) from sub-surface geophysical data concluded that the fault zone contains a major thrust component. This might be due to Pennsylvanian-age inversion of the older early Cambrian normal faults (Tapp, 1995) of the southern Oklahoma fault system of Thomas (1993).

DESCRIPTION OF THE OUTCROPS

Outcrop 1: Second-order folds and a conjugate set of reverse faults in the southern limb of the Arbuckle anticline

The first outcrop is located in the southern limb of the Arbuckle anticline where second-order upright folds and a conjugate set of reverse faults are exposed along the road cut of I-35 (Figures 2-4). These structures deform the Lower Ordivician West Spring Creek and the Kindblade formations dominated by massive beds of grey limestone with minor black chert modules. The folds are a gentle anticline in the south and an open syncline to the north. The axes of both folds are shallowly plunging to the west. The anticline is deformed by reverse faults moderately to steeply dipping to the south and north.

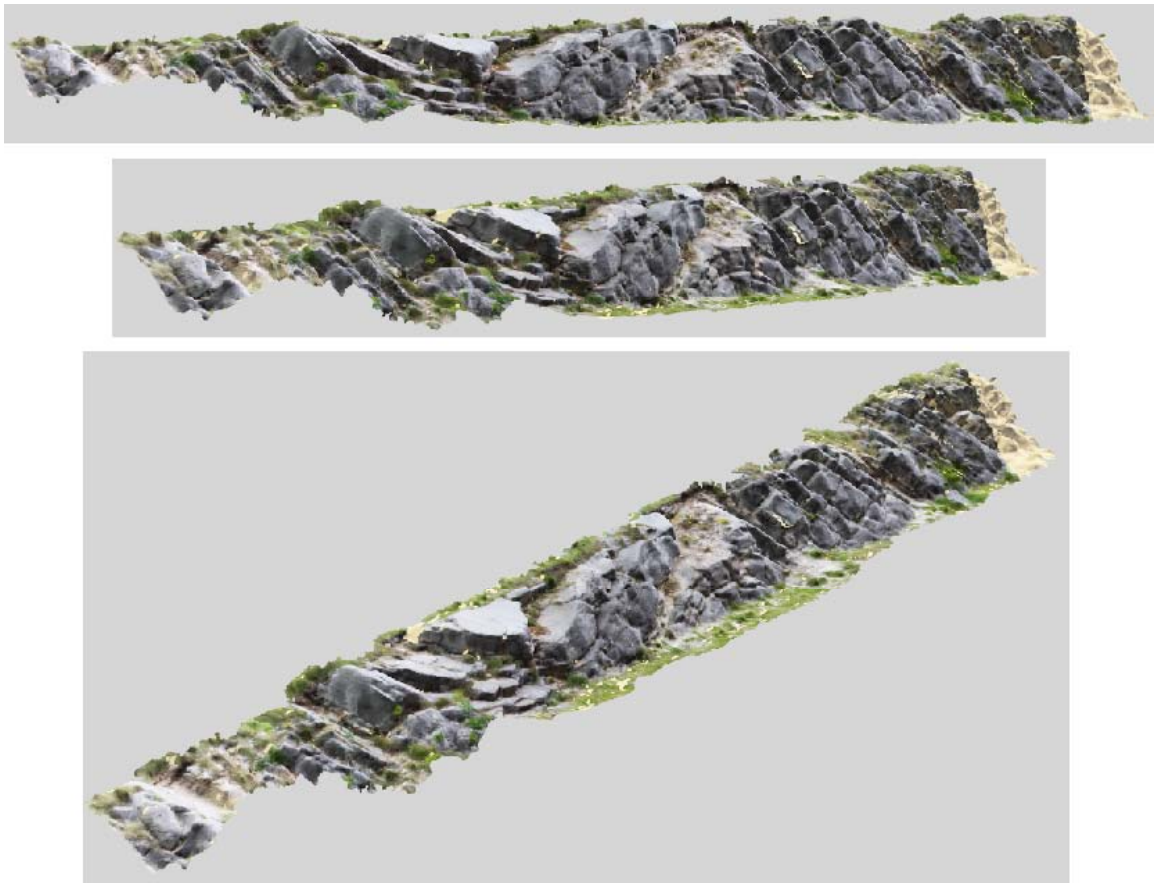

Figure 3: The 3DR model of outcrop 1 viewed from different directions. Please note that the model have a dynamic compass that points to north, east and vertical when viewed as OpenSceneGraph or 3D PDF file. It also contains a measurement tool for scale.

Outcrop 2: Second-order folds and thrusts on the hinge of the Arbuckle anticline

The second outcrop exposes second-order folds, thrusts, and normal folds on the hinge of the Arbuckle anticline along I-35 (Figure 2, 5 and 6). These structures deform the Upper Cambrian limestone and dolomite of the Timbered Hill group and the Butterly dolomite which occur as massive to thin beds. The central part of the outcrop is dominated by N-verging folds with uniform axes that plunge shallowly to the west. The fold axial surfaces of these folds as well as mesoscopic thrusts dip moderately to the south. However, in the northern part of the outcrop the folds become more upright with nearly vertical fold axial surfaces, although the fold axes of these folds plunge shallowly to the west similar to

Figure 4: Close-up of the 3DR model of outcrop 1.

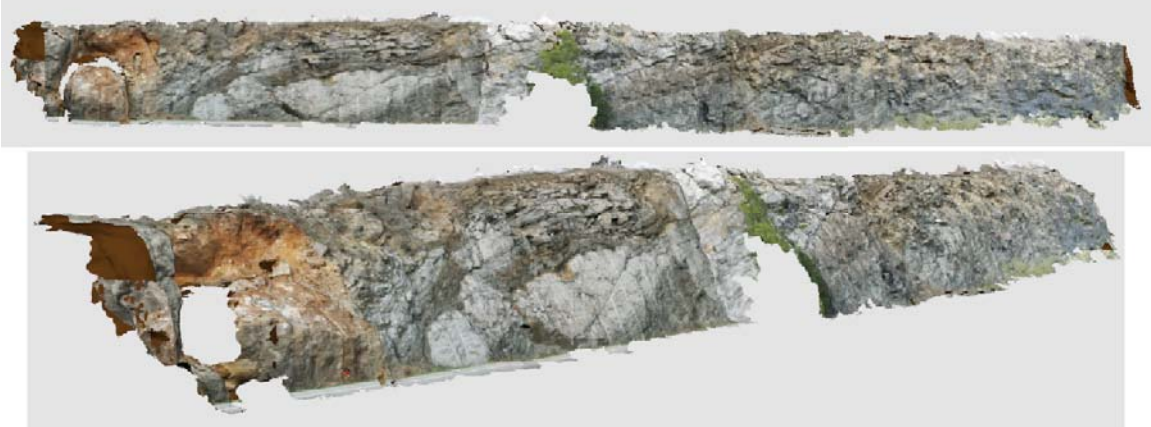

Figure 5: The 3DR model of outcrop 2 viewed from different directions.

those of the N-verging folds in the central part of the outcrop. Hence, the development of these folds are interpreted as due to co-axial, but non co-planar deformation accompanied the top-to-the-north movement across the Chapman Ranch thrust south of the Arbuckle anticline hinge zone (Figure 2). No second-order folds or thrusts are observed in the southern part of the outcrop. Rather, a set of N- and S-dipping normal faults are observed where they deform the massive beds of the Timbered Hill group and the Butterly dolomite.

Outcrop 3: An angular unconformity in the northern limb of the Arbuckle anticline

The third outcrop represents part of the Washita Valley fault zone along I-35 where the sub-horizontal beds of the Pennsylvanian-age Collings Ranch conglomerate overly the variably dipping beds of the Middle-Upper Ordovician-age Sylvan shale and the Viola group forming a classical angular unconformity observed in the southern part of the outcrop (Figures 7 and 8). The northernmost part of outcrops is dominated by deeply weathered S-dipping thin beds of the Sylvan shale conformably overlain by the thin

Figure 6: Close-up of the 3DR model of outcrop 2.

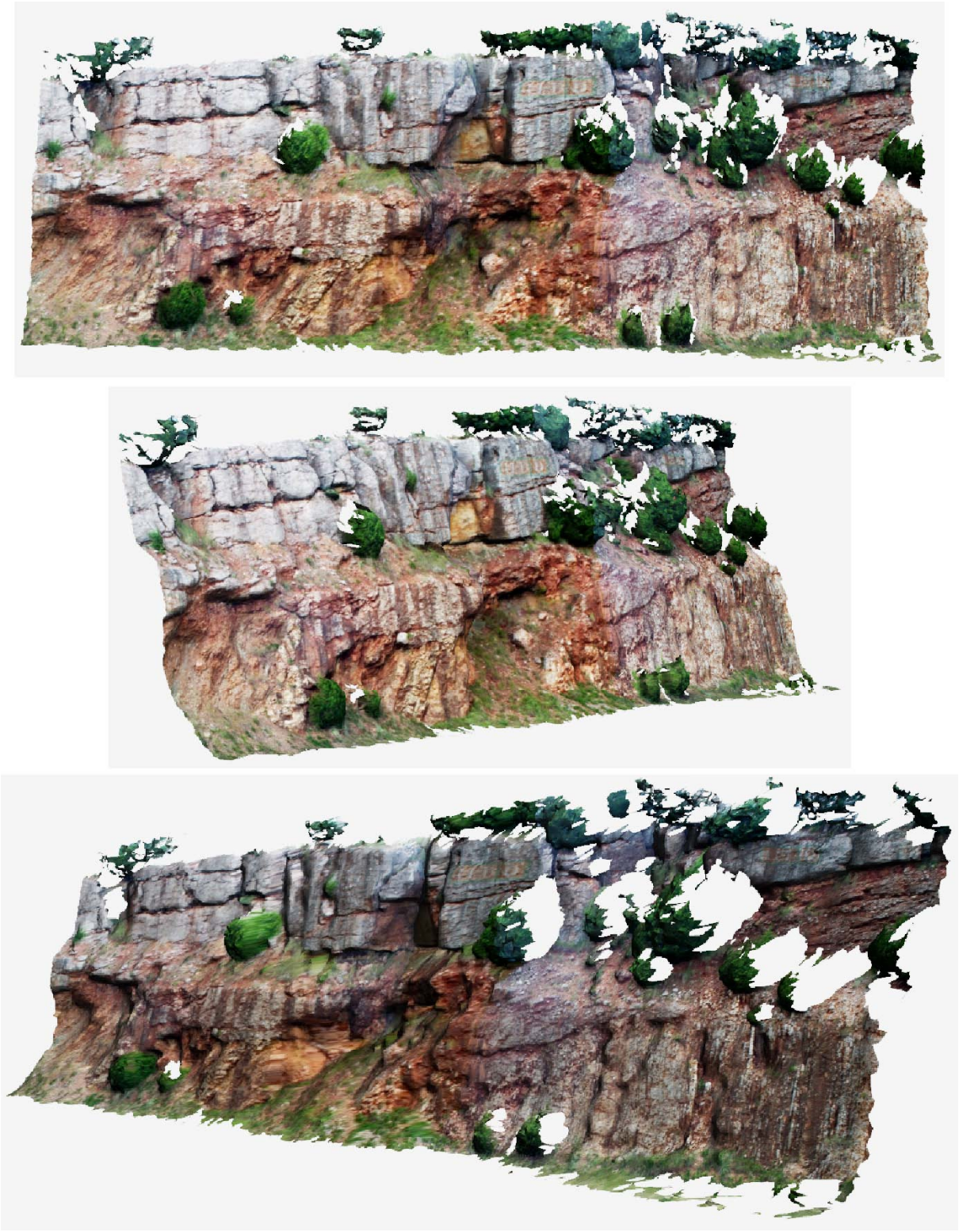

Figure 7: The 3DR model of outcrop 3 viewed from different directions.

Figure 8: Close-up of the 3DR of outcrop 2.

limestone beds of the Viola group. The trend of the Viola group beds become more horizontal southward, then N-dipping and vertical towards the southern end of the outcrop. The variation in the trend of the Viola group limestone is interpreted as defining a broad syncline. This fold is dissected by numerous NW-trending steep faults, the fault planes of which contain sub-horizontal slickenlines (defined by fibrous calcite) indicating the dominance of strike-slip component in this part of the Washita Valley fault zone. Additionally, minor normal-slip displacements are observed along the vertical limestone beds of the Viola group where the sub-horizontal beds of the Collings Ranch conglomerate overly them. These are interpreted as due to activation of the bedding planes as normal faults due to loading imposed by the overlying Collings Ranch conglomerate.

TEACHING MODULES

Module 1: Viewing the outcrops to show various geological structures

The following steps can be used to view the three 3DR models: (1) Click on the icons labeled Outcrop Number 1, Outcrop Number 2, or Outcrop Number 3 to start viewing the models in 3D using Adobe Acrobat Pro. (3) When the model appears on Adobe Acrobat Pro, click on it to activate 3D viewing and manipulation. (3) You can rotate the model and zoom-in and out at this stage, but it is preferred that you view the model in full screen. To do that hold down the mouse right button anywhere in the model and activate “Full Screen Multimidia”. (4) Holding down the left button of the computer mouse and moving the mouse laterally will allow you to rotate the model horizontally. On the other hand, up and down movement will allow you to rotate the model vertically. (5) Holding

down the right button of the computer mouse and moving the mouse laterally will allow you to zoon-in and out. (6) Holding down both buttons and moving the mouse laterally or up and down will allow moving the entire model and position it anywhere in the screen. (7) The dynamic compass in the lower left part of the model gives the north, east and vertical directions. However, not to lose track of the model orientation, it is preferred that every now and then to click on the model using the left button to display the reference frame (Figure 9). Clicking the left button anywhere on the screen, expect the model itself, will allow exiting the reference frame mode. Distances can be measured using "Tools-Analysis-Measuring Tool" function (Figure 9).

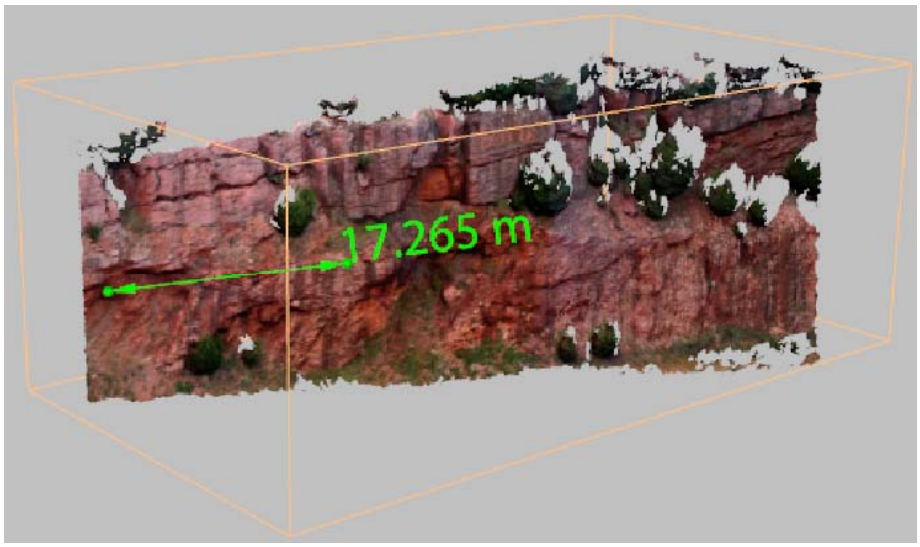

Figure 9: reference frame and measurement of the 3DR models.

The three 3DR models contain a number of geological structures that can be shown to the students through a virtual field trip:

(1) Outcrop 1 provides the opportunity to show dipping bedding planes, an anticline, a syncline, and a reverse fault (Figure 10).

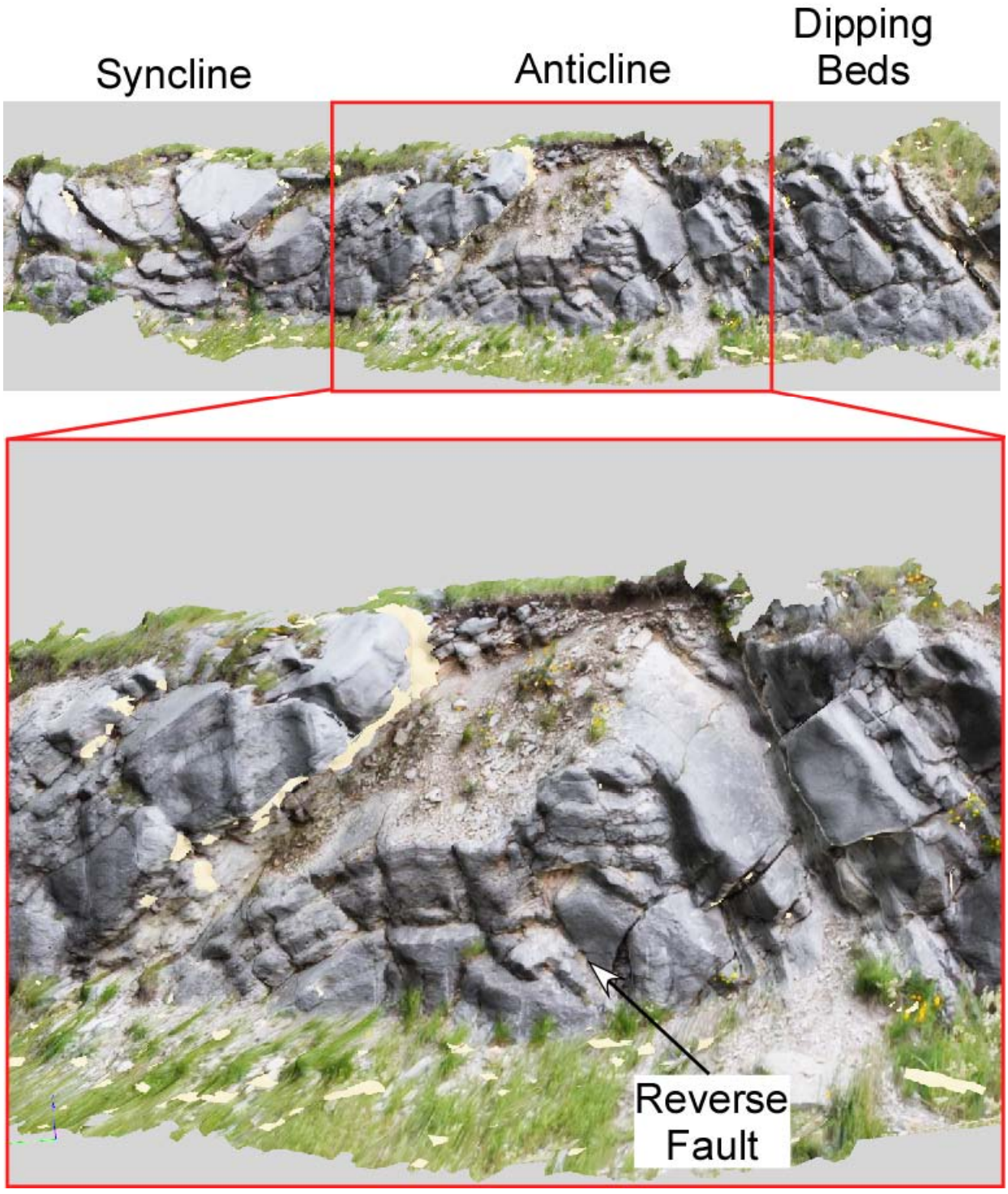

Figure 10: Some of the structural features that can be viewed by students in the 3DR model of outcrop 1. Please note that, when zooming-in, both the PDF and OpenSceneGraphs of the model provides a much better spatial resolution that what is displayed in this figure.

(2) There are numerous mesoscopic structural features that can be shown in Outcrop 2 including a normal fault, a fault termination, a thrust fault and a frontal ramp (Figure 11).

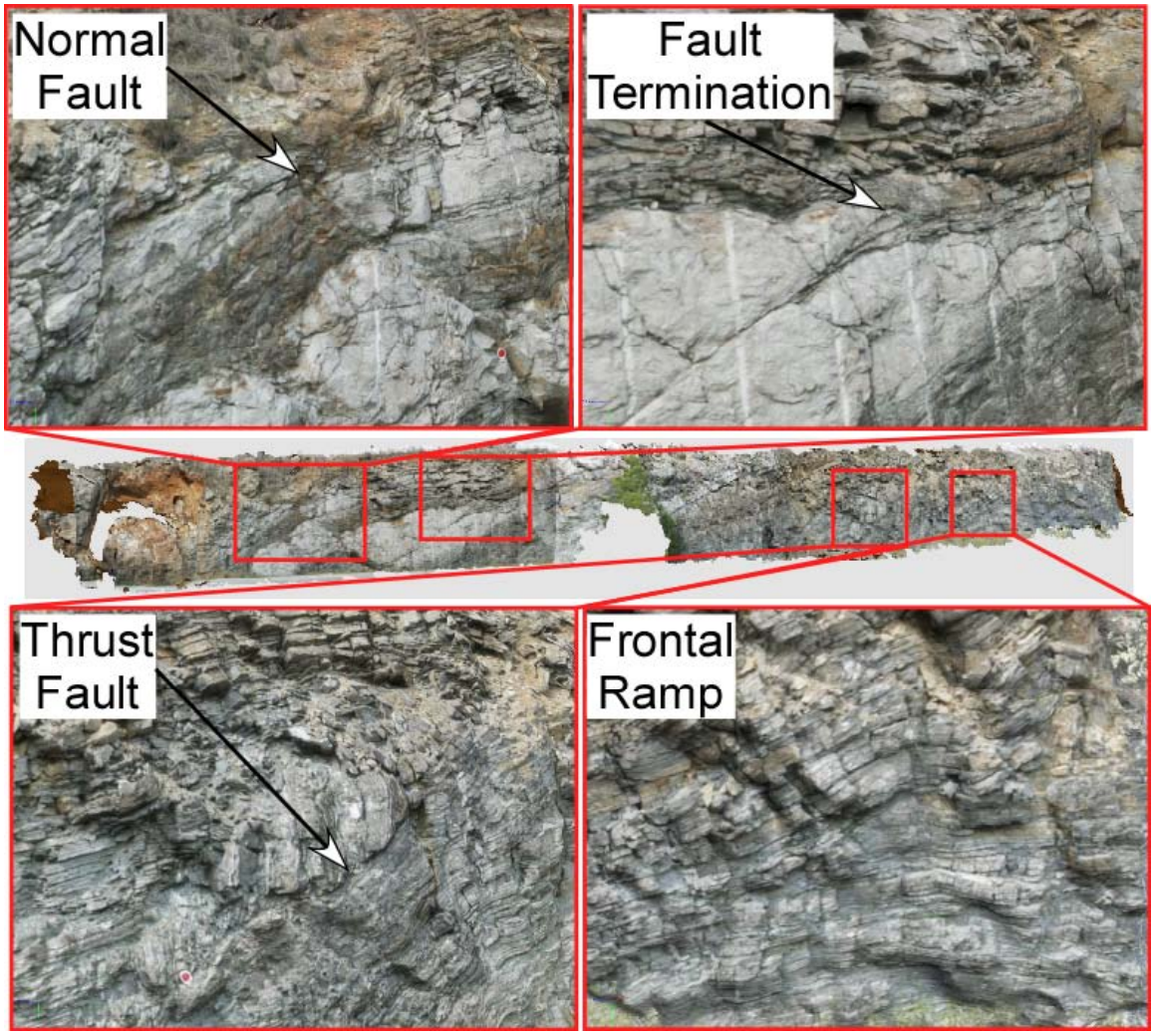

Figure 11: Some of the structural features that can be viewed by students in the 3DR model of outcrop 2. Please note that, when zooming-in, both the PDF and OpenSceneGraphs of the model provides a much better spatial resolution that what is displayed in this figure.

(3) Outcrop 3 can be used to show an angular unconformity (Figure 12).

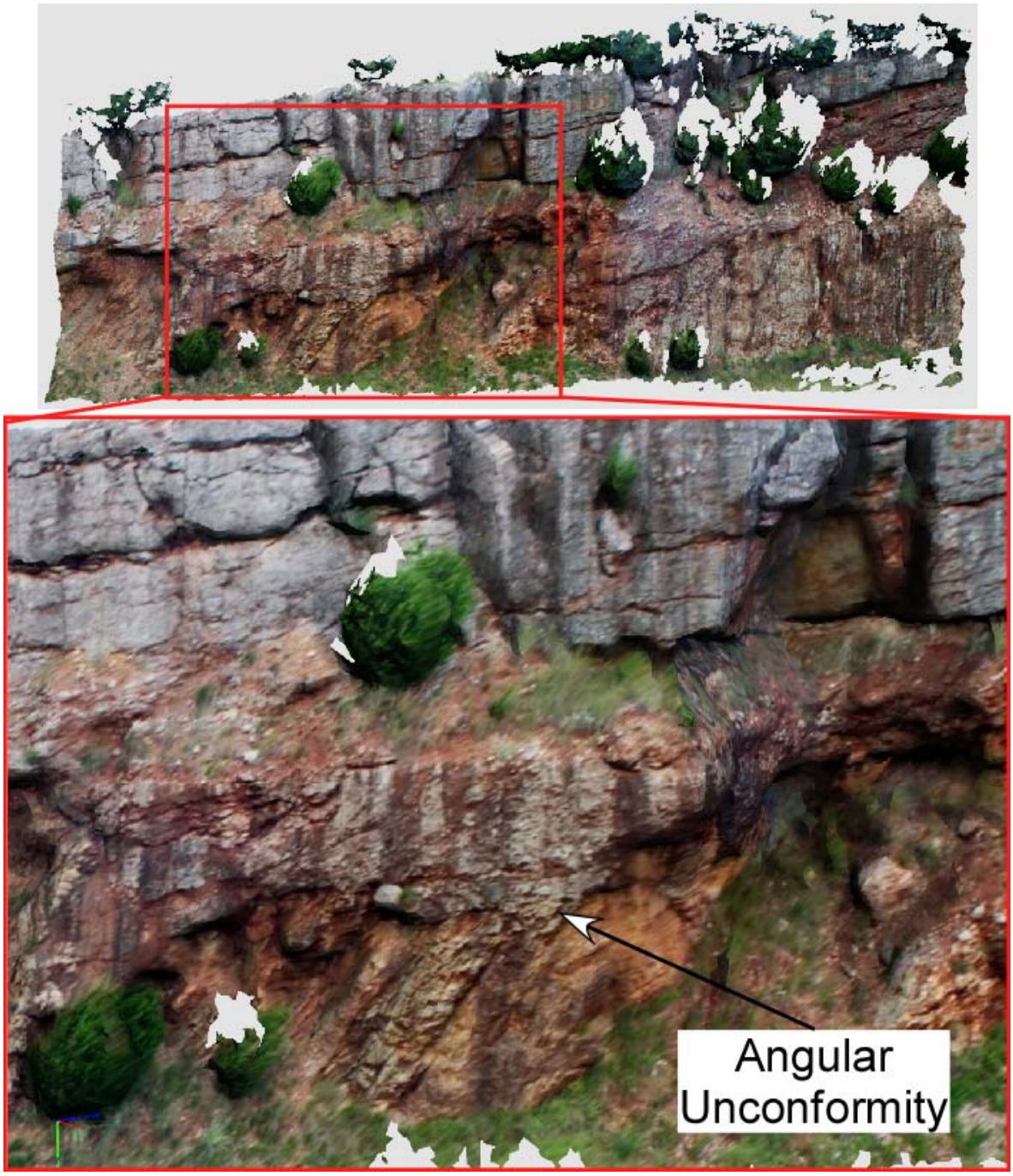

Figure 12: Some of the structural features that can be viewed by students in the 3DR model of outcrop 2. Please note that, when zooming-in, both the PDF and OpenSceneGraphs of the model provides a much better spatial resolution that what is displayed in this figure provides.

Module 2: Strike Lines

Outcrop 1 can be used to explain the concept of strike line (Figures 13 and 14). This can be accomplished as follows. (1) The students manipulate the model and examine different bedding planes. (2) The model is then rotated to its actual north-east-vertical orientation. A close-up view of the 3DR model can be captured and imported into any digital drawing software such as Canvas or Adobe Illustrator. Holding down “Ctrl and Alt” and clicking “PrtScn” will allow capturing the screen shoot and importing it into the drawing software. (3) Tracing the southern limb of the anticline. (4) Horizontal lines at equal elevation intervals are drawn on the fold limb. (5) These lines are then projected to the horizontal plane. (6) The students will realized that the spacing of the strike lines increases as the bedding plane become shallower. The students will also realized that as the hinge of the anticline is reached the distance between strike lines become infinite.

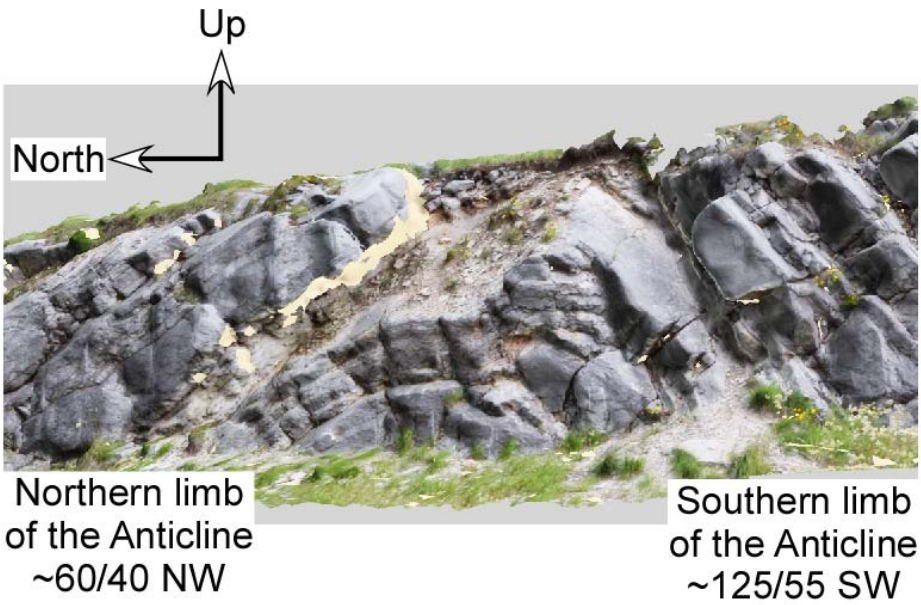

Figure 13: Positioning outcrop 1 to its actual orientation. Please note that the dynamic compass in the OpenSceneGraph and the 3D PDF files will help you orienting the 3DR model of the outcrop.

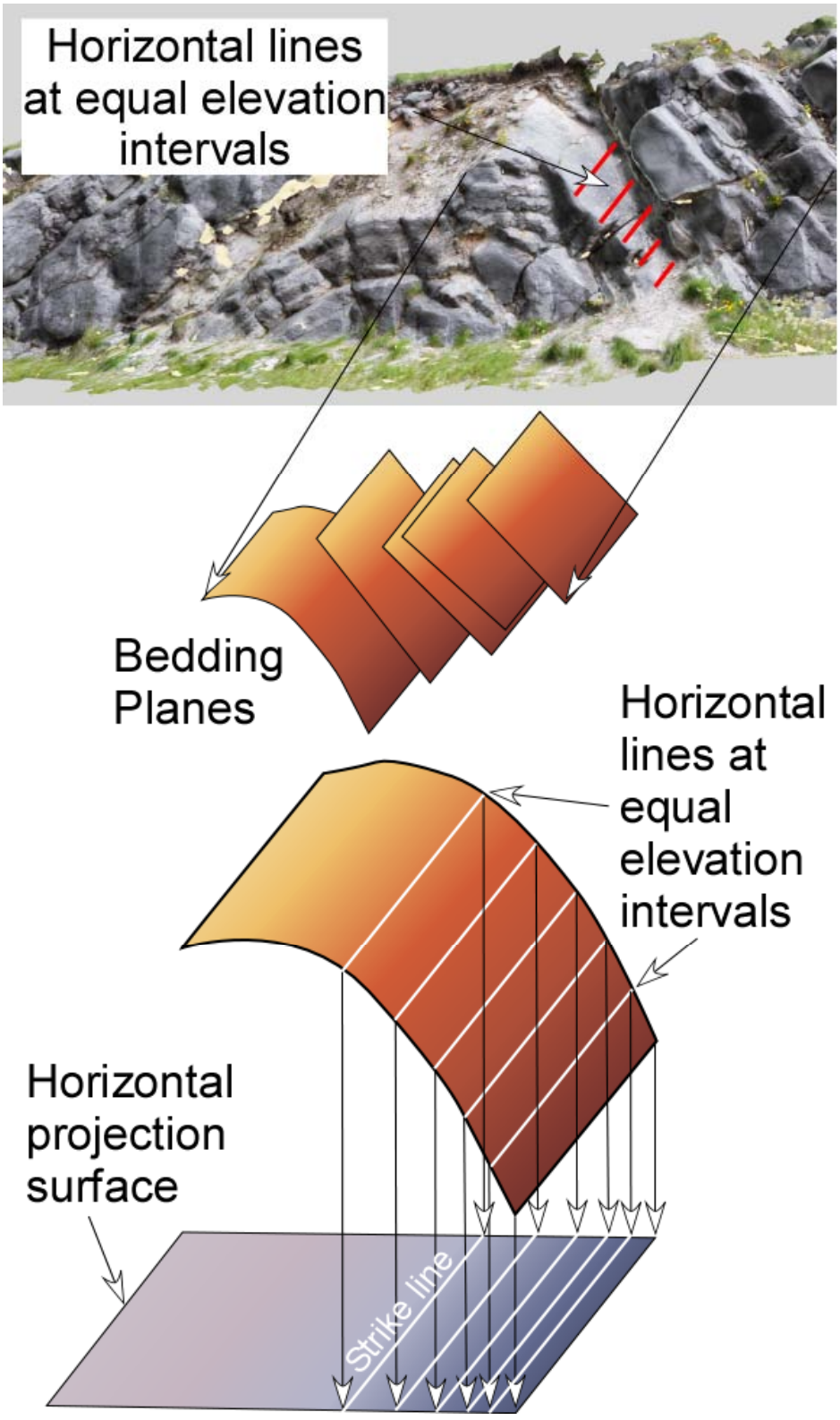

Figure 14: Explaining the concept of strike lines using outcrop 1.

Module 3: Fold Geometry, relationship between folding and faulting, and Strain Analysis

Outcrop 1 also provides opportunities to examine fold geometry, relationship between folding and folding, and strain analysis (Figure 15). The outcrop exposes a syncline in the north and an anticline to the south. This module focuses on the anticline which is an upright (strike and dip of the fold axial surface is $95^{o}/85^{o}$N), gentle (inter-limb angle is 120^{o}), W-plunging structure (trend and plunge of the fold axis is $294^{o}/22^{o}$). The hinge zone of the anticline is dissected by E-W trending reverse faults that are dipping north and south (Figure 15). (1) The students manipulate the model and examine the fold and the fault. (2) The model is then rotated to its actual north-east-vertical orientation. (3) Importing the 3DR model into the drawing software. (4) The faults deforming the anticline can be traced. (5) Different bedding planes defining the anticline are subsequently traced and given different colors. The students will realize that bedding planes are offset to define reverse faults. (6) The students will be asked to draw a strain ellipsoid that explains the relationship between folding and faulting. Since the fold axial surface of the fold strikes E-W and it is upright, it safe to assume that the anticline was the result of N-S directed shortening. As shortening continued, the reverse faults were formed as zones of high shear strain within an overall pure shear strain. (7) By comparing the undeformed state (circle) and the deformed state (ellipse) the students can be asked which lines are shortened, elongated, or remained unchanged. The students are expected to realize that the lines representing the zones of high shear strain remained unchanged.

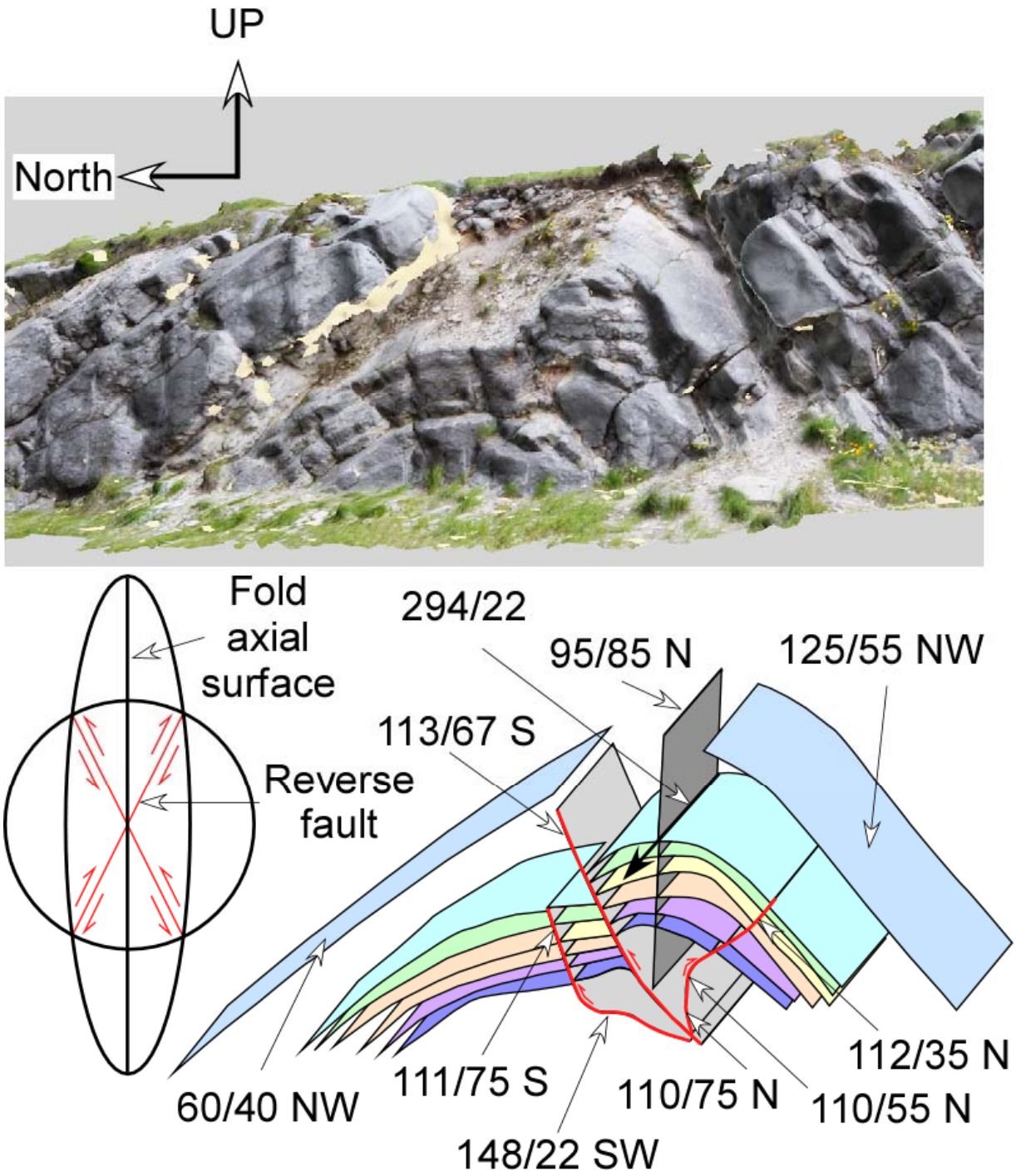

Figure 15: Explaining fold geometry, relationship between folding and faulting and strain analysis.

Module 4: Relationship between folding and thrusting and cross-section restoration

Outcrop 2 can be used to examine the relationship between folding and thrusting and restore the section to its un-deformed state (Figure 16). This outcrop shows a number of dominantly N-verging asymmetrical folds and thrusts. The axial surfaces of these folds dip to the southwest but the dip angle increases northward. The axes of these folds, on the other hand, do not show any variation in their trend and plunge indicating co-axial but non co-planar deformation. Restoring the section to its un-deformed state will allow the students to calculate the amount of shortening occurred during folding and thrusting. (1) The students manipulate the model and examine different folds and thrusts. (2) The model is then rotated to its actual north-east-up orientation. (3) Importing the 3DR model into the drawing software. (4) The students can then trace a single marker horizon (bedding plane) that define the geometry of the folds, it is offset by the thrust, and it can be traced throughout the length of the model. (5) The students can then restore the section to its pre-thrusting state. (6) Subsequently, the students can un-fold the section. (6) Finally, the length of the deformed and un-deformed section can be measured and the amount of shortening can be calculated. In this part of outcrop 3 the amount of shortening is ~30%.

ACKNOWLEDGEMENTS

This work is supported by a National Science Foundation (NSF) – Course, Curriculum and Laboratory Improvement (CCLI) program through a project entitled “Cyber-mapping for Teaching Undergraduate Geosciences Courses” (Award number 0719816).

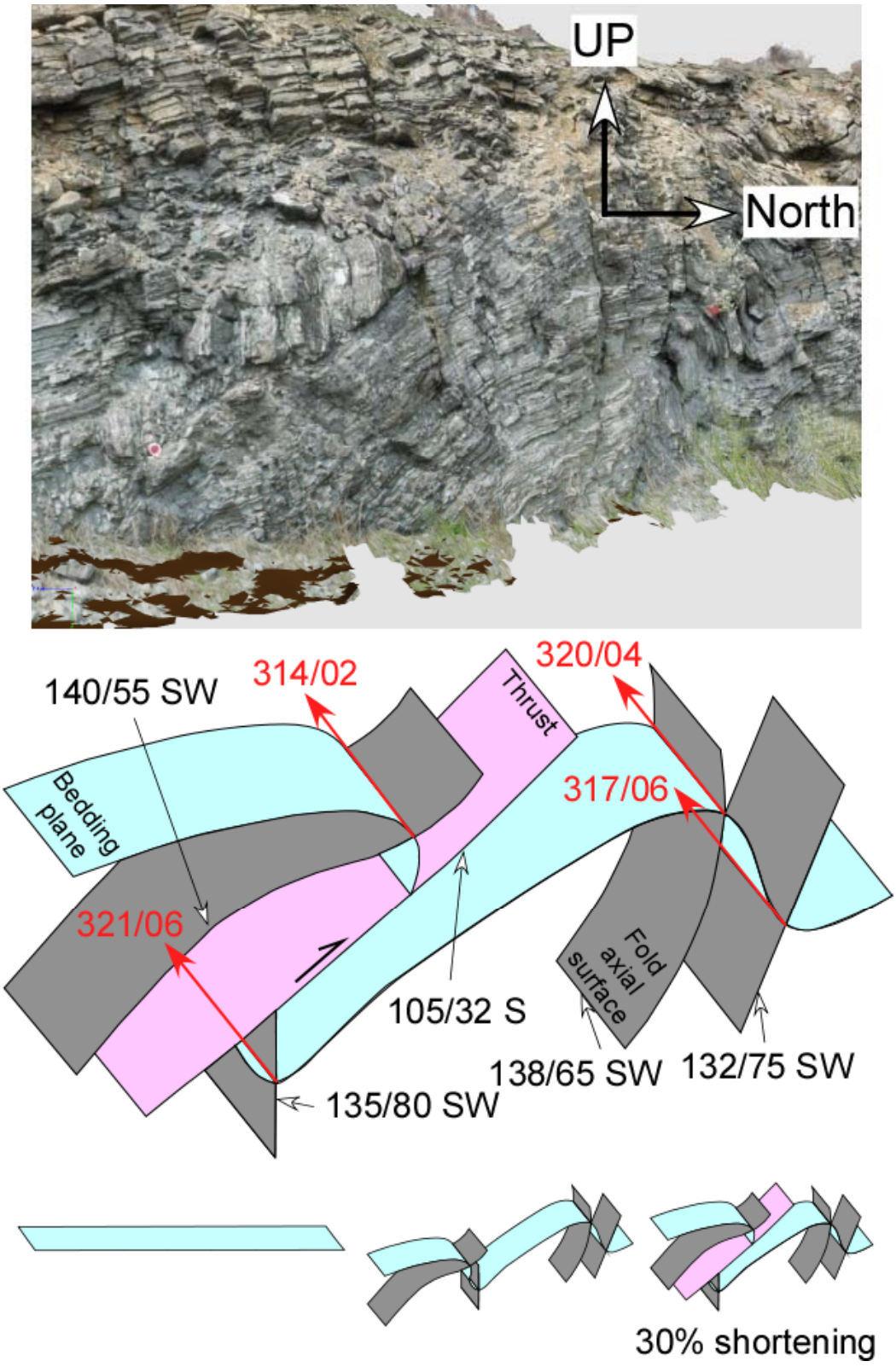

Figure 16: Analysis of outcrop 2 to calculate amount of shortening

REFERENCES

Alfarhan, M. 2010. Geosciences Information System (GeoIS): A geospatial paradigm for real and virtual 3D worlds. Ph.D. Dissertation. University of Texas at Dallas, Richardson, Texas. 114 p.

Alfarhan, M., White, L., Tuck, D., and Aiken, C. 2008. Laser rangefinders and ArcGIS combined with three-dimensional photorealistic modeling for mapping outcrops in the Slick Hills, Oklahoma. Geosphere, 4, 576-587.

Bellian, J.A., Kerans, C., And Jennette, D.C., 2005, Digital outcrop models: Applications of terrestrial scanning LiDAR technology in stratigraphic modeling: Journal of Sedimentary Research. 75, 166-176.

Edelson, D.C., and Gordin, D. 1998. Visualization for learners: A framework for adapting scientists' tools. Computers and Geosciences. 24, 607-616.

Geological map and sections of the Arbuckle mountains, Oklahoma. By: Ham, W.E., and McKinley, M.E. (1954). Revised by Johnson, K.S. (1990). Published by the Oklahoma Geological Survey.

Hurst, S. D. 1998. Use of "virtual" field trips in teaching introductory geology. Computer and Geosciences. 24, 653-659.

Johnson, A., Morin, P., and Van Keken, P. 2006. GeoWall: Stereoscopic visualization for geosciences research and education. Applications – IEEE Computer Society, November-December issue, 10-14.

Kelly, M.M., and Riggs, N.R. 2006. Use of virtual environment in the GeoWall to increase student confidence and performance during field mapping: An example from an introductory-level field class. Journal of Geoscience Education 54, 158-164.

Kemp, E.A.D. 1999. Visualization of complex geological structures using 3-D Bézier construction tools. Computers and Geosciences. 25, 581-597.

Marschallinger, R and Johnson, S.E. 2001. Presenting 3-D models of geological materials on the World Wide Web. Computer and Geosciences. 27, 467-476.

McCaffrey, K.J.W., Jones, R.R., Holdsworth, R.E., Wilson, R.W., Clegg, P., Imer, J., Holliman, N., and Trinks, I. 2005. Unlocking the spatial dimension: Digital technologies and the future of Geoscience fieldwork. Journal of the Geological Society, London. 162, 1-2.

Olariu, I., Ferguson, J., and Aiken, C. 2008. Outcrop fracture characterization using terrestrial laser scanners, deepwater Jackfork Sandstone at Big Rock Quarry, Arkansas. Geosphere. 4, 247-259.

Oldow, J.S., Walker, J.D., Aiken, C.L.V., And Xu, X., 2006, Digital acquisition, analysis, and visualization in the earth sciences. Eos (Transactions, American Geophysical Union) 87, 351.

Palladino, D.L. 1986. Structural analysis of a portion of the Washita Valley fault zone, Arbuckle mountains, southern Oklahoma. M.S. thesis. Baylor University, Waco, TX. 150p.

Parkinson, B.W., Spilker, J.J. 1996. Axelrad, P., and Enge, P. Global Positioning System: Theory and applications, Volume II. Progress in Astronautics and Aeronautics. 164, 627 p.

Pringle, J.K., Howell, A., Hodgetts, D., Westerman, A.R., and Hodgson, D.M. 2006. Virtual outcrop models of petroleum reservoir analogues: A review of the current state of-the-art. First Break. 24, 33-42

Tanner III, J.H. 1967. Wrench fault movement along Washita Valley Fault, Arbuckle Mountain Area, Oklahoma: Geological Notes. American Association of Petroleum Geologists Bulletin. 51, 126-134.

Tapp, B. 1995. Inversion model for the structural style of the Arbuckle region. In: Johnson, K.S. Structural styles of the southern Midcontinent, 1992 symposium, Oklahoma Geological Survey Circular 97, 113-118.

Thomas, W.A. 1993. Low-angle detachment geometry of the late Precambrian-Cambrian Appalachian-Ouachita rifted margin of southeastern North America. Geology. 21, 921-924.

Thomas, W.A. 2004. Genetic relationship of rift-stage crustal structure, terrane accretion, and foreland tectonics along the southern Appalachian-Ouachita orogen. Journal of Geodynamics 37, 549-563.

Thurmond, J., Drzewiecki, P.A., and Xu, X. 2005, Building simple multi-scale visualizations of outcrop geology using virtual reality modeling language (VRML). Computers and Geosciences. 31, 913-19.

Wilkinson, R.P. 1997. Is the Washita Valley fault a strike-slip fault or a thrust fault, and who cares? In: McMahan, G. Transactions of the 1997 American Association of Petroleum Geologists Midcontinent Section Meeting. Oklahoma City Geological Society, 94-98.

Xu, X. 2000. 3D virtual geology; Photorealistic outcrops and their acquisition, visualization and analysis. Ph.D. Dissertation. University of Texas at Dallas, Dallas, Texas. 169 p.

Xu, X., Aiken, C., and Nielsen, K.S. 1999. Real time and the virtual outcrop improve geological field mapping. Eos (Transactions, American Geophysical Union). 80, 317, 322–324.

Xu, X., Aiken, C., Bhattacharya, J.R., Corbeanu, R.M., Nielsen, K.C., McMechan, G.A., and Abdelsalam, M.G. 2000. Creating virtual 3-D outcrop: Leading Edge.19, 197-202.

Xu, X., Bhattacharya, J., Davies, R.K., and Aiken, C.L.V. 2001. Digital geologic mapping of the Ferron Sandstone, Muddy Creek, Utah with GPS and reflectorless laser Rangefinders. GPS Solutions. 5, 15-23.

Xu, X., Aiken, C., Thurmond, J., and Nuebert, B. 2004. Beyond point clouds: The future of 3D virtual models. Geoworld, 38-41.

Zeng, X., McMechan, G.A., Bhattacharya, J.P., Aiken, C.L.V., Xu, X., Hammon, W.S., and Corbeanu, R.M. 2004. 3-D imaging of a reservoir analog in point bar deposits in the Ferron Sandstone, Utah, using ground-penetrating radar. Geophysical Prospecting. 52, 151-163.